Heliyon 10 (2024) e24865

Contents lists available at ScienceDirect

Heliyon

journal homepage: www.cell.com/heliyon

Research article

Network pharmacology, molecular docking, combined with experimental verification to explore the role and mechanism of shizhifang decoction in the treatment of hyperuricemia

Zhiyuan Wu [a,b,c,d], Chuanxu Wang [a,b,c,d], Feng Yang [a,b,c,d], Jiabao Zhou [a,b,c,d], Xuming Zhang [a,b,c,d], Jiadong Xin [a,b,c,d], Jiandong Gao [a,b,c,d,*]

[a] Department of Nephrology, Shuguang Hospital Affiliated to Shanghai University of Traditional Chinese Medicine, Shanghai, China
[b] TCM Institute of Kidney Disease, Shanghai University of Traditional Chinese Medicine, Shanghai, China
[c] Key Laboratory of Liver and Kidney Diseases, Ministry of Education, Shanghai University of Traditional Chinese Medicine, Shanghai, China
[d] Shanghai Key Laboratory of Traditional Chinese Clinical Medicine, Shanghai University of Traditional Chinese Medicine, Shanghai, China

ARTICLE INFO

Keywords:
ERK1/2 signaling pathway
Cell apoptosis
Hyperuricemia
Network pharmacology
Molecular docking
Mechanism research

ABSTRACT

Ethnopharmacological relevance: Shizhifang Decoction, a traditional Chinese medicine prescription formulated by Professor Zheng Pingdong of Shuguang Hospital, has been widely utilized in clinical settings for the treatment of hyperuricemia due to its proven safety and efficacy.
Objective: In this study, we used network pharmacology, molecular docking technology, and experimental validation to elucidate the therapeutic effects and underlying mechanisms of Shizhifang Decoction in managing hyperuricemia.
Methods: Quality control and component identification of the freeze-dried powder of Shizhifang Decoction were conducted using ultra-high performance liquid chromatography-tandem quadrupole time-of-flight mass spectrometry. Active ingredients and their corresponding targets were obtained from Traditional Chinese Medicine Systems Pharmacology, Traditional Chinese Medicine Information Database, The Encyclopedia of Traditional Chinese Medicine, and other databases. Disease-related targets for hyperuricemia were collected from GeneCards and DisGeNET databases. The Venny platform is used to screen common targets for drug active ingredients and diseases. Subsequently, we constructed an active component-target-disease interaction network using the Search Tool for the Retrieval of Interacting Genes/Proteins (STRING) database, create a component disease common target network using Cytoscape 3.9.1 software, from which core targets were selected. Import common targets into the Database for Annotation, Visualization and Integrated Discovery (DAVID) for Gene Ontology enrichment and Kyoto Encyclopedia of Genes and Genomes pathway analysis. Molecular docking was then conducted to validate the binding capacity of key active ingredients and their associated targets in Shizhifang Decoction. The theoretical predictions were further confirmed through in vitro and in vivo experiments.
Result: A total of 35 active ingredients and 597 action targets were identified, resulting in 890 disease-related targets for hyperuricemia. After comprehensive analysis, 99 common targets were determined. Protein-protein interaction network analysis revealed crucial relationships between these targets and hyperuricemia. Among them, 12 core targets (CASP3, IL1B, IL6, TNF, TP53, GAPDH, PTGS2, MYC, INS, VEGFA, ESR1, PPARG) were identified. Gene Ontology enrichment

* Corresponding author. Department of Nephrology, Shuguang Hospital Affiliated to Shanghai University of Traditional Chinese Medicine, Shanghai, China.
E-mail address: jiandong.gao@shutcm.edu.cn (J. Gao).

https://doi.org/10.1016/j.heliyon.2024.e24865
Received 22 June 2023; Received in revised form 12 October 2023; Accepted 11 January 2024
Available online 25 January 2024

analysis demonstrated significant associations with the regulation of inflammatory response, cell apoptosis, and the positive regulation of extracellular regulated protein kinases 1 and extracellular regulated protein kinases 2 cascades. Kyoto Encyclopedia of Genes and Genomes pathway analysis highlighted inflammation and apoptosis-related pathways as critical mediators of Shizhifang Decoction's effects on hyperuricemia. Molecular docking studies further supported the interactions between apoptosis-related proteins and active ingredients in the extracellular regulated protein kinases 1/2 signaling pathway. In vitro experiments confirmed the downregulation of apoptosis-related proteins (caspase-3, Bax, Bcl-2) and the inhibition of the extracellular regulated protein kinases 1/2 signaling pathway by Shizhifang Decoction. These findings were also validated in animal models, demonstrating the potential of Shizhifang Decoction to mitigate renal injury induced by hyperuricemia through extracellular regulated protein kinases 1/2-mediated inhibition of renal tubular epithelial cell apoptosis.

Conclusion: Our study provides valuable insights into the main mechanism by which Shizhifang Decoction ameliorates hyperuricemia. By targeting the ERK1/2 signaling pathway and modulating cell apoptosis, Shizhifang Decoction exhibits promising therapeutic potential for the treatment of hyperuricemia. These findings support the continued exploration and development of Shizhifang Decoction as a potential herbal remedy for hyperuricemia management.

Abbreviations

AGE-RAGE	Advanced glycation end products -receptor for advanced glyca-tion end products
BJ	Sinapis alba
CC	Cellular components
CQ	Plantago asiatica L
DL	Drug similarity
DC	Degree value
DK	Semen malvae verticillatae
ERK1/2	Extracellular regulated protein kinases 1/2
GO	Gene ontology
HUA	Hyperuricemia
HK-2	Human renal cortex proximal convoluted tubule epithelial cells
HE	Hematoxylin-eosin staining
HIF	Hypoxia Inducible Factor
IL-17	Interleukin-17
KEGG	Kyoto Encyclopedia of Genes and Genomes
LX	Vaccariae Semen
MF	Molecular functions
Masson	Masson's Trichrome Staining
MAPK	Mitogen-activated protein kinase
SZF	Shizhifang decoction
SPF	Specific Pathogen-Free
OA	Potassium oxoxazine
OB	Oral availability
PPI	Protein-protein interaction
PAS	Schiff periodic acid shiff
PI3K-Akt	Phosphatidylinositol 3 kinase-protein kinase B
UA	Uric acid
SPSS	Statistical Product and Service Solutions
TNF	Tumor necrosis factor

1. Introduction

Uric acid is a byproduct of purine metabolism in the human body. Abnormal uric acid metabolism will lead to increased uric acid in the blood and hyperuricemia (HUA) [1]. Hyperuricemia is a significant metabolic disorder closely associated with cardiovascular disease, diabetes, and gout [2]. Furthermore, impaired uric acid metabolism, mainly metabolized by the kidneys, can lead to kidney diseases and, in severe cases, progress to end-stage kidney disease. Existing research suggests that high uric acid levels can directly damage proximal renal tubules, potentially through the promotion of renal tubular cell apoptosis by uric acid [3,4]. Despite the use of

first-line drugs like febuxostat and allopurinol in clinical practice to treat hyperuricemia, reports on their side effects persist [5]. Traditional Chinese medicine offers a notable advantage with fewer side effects and has demonstrated efficacy in the treatment of hyperuricemia. Studies have found that the ethanol extract of Sanghuangporus vanini can inhibit renal tubular epithelial cell apoptosis and alleviate kidney injury induced by HUA [6]. Additionally, renal herb formulas have been shown to prevent hyperuricemia nephropathy by inhibiting apoptosis and inflammation [7]. Therefore, it is necessary to explore the treatment of traditional Chinese medicine [8]. Shizhifang Decoction (SZF) is an empirically formulated prescription used to treat hyperuricemia at Shuguang Hospital affiliated with Shanghai University of Traditional Chinese Medicine. It comprises standardized herbal medicines such as *Plantago asiatica* L, *Sinapis alba* L, *Maklva verticillata* L, and *Gypsophila vaccaria (L.) Sm*. All names of Chinese herbal medicines have passed through "The World Flora Online" (http://www.worldfloraonline.org) Standardize. SZF has been shown to effectively reduce uric acid levels and alleviate kidney damage caused by hyperuricemia [9,10]. Previous research by our research group has demonstrated that SZF can inhibit the activation of reactive oxygen species in rat kidney mitochondria, thereby reducing renal tubular injury and inflammation [10]. Furthermore, recent studies indicate that SZF can mitigate pyroptosis of renal tubular epithelium. These findings collectively suggest that SZF exerts its therapeutic effects through multiple pathways, targets, and mechanisms [11]. Network pharmacology is a valuable approach to explore the potential mechanisms of traditional Chinese medicine prescriptions by utilizing existing databases to elucidate the impact of drugs on diseases [12]. In this study, we employed network pharmacology to identify the active components of SZF, construct an interaction network between SZF and hyperuricemia target proteins, select key targets and related pathways, and validate the binding ability of important targets determined by network pharmacology with key active components through molecular docking. Lastly, we verified the network pharmacology predictions through experiments, providing a solid theoretical and research foundation for understanding the mechanism of SZF in treating hyperuricemia.

2. Materials and methods

2.1. Herbs of SZF decoction

The SZF dry powder consisted of the following herbs: 30 g of *Plantago asiatica* L (production batch number 181127, Jiangxi, China), 15 g of *Sinapis alba* (production batch number 180907, Zhejiang, China), 15 g of *Vaccariae Semen* (production batch number 181129, Hebei, China), and 15 g of *Semen malvae verticillatae* (production batch number 180915, Zhejiang, China). The dry extract powder was prepared by Shanghai Traditional Chinese Medicine Pharmaceutical Technology Service Co., Ltd., upon commission from Shuguang Hospital affiliated with Shanghai University of Traditional Chinese Medicine. These were determined by Director Liu Li of the Pharmacy Department of Shuguang Hospital, Shanghai University of Traditional Chinese Medicine. The metabolic components of SZF freeze-dried powder were analyzed using ultra-high performance liquid chromatography quadrupole time-of-flight mass spectrometry (UPLC-Q-TOF-MS/MS).

2.2. Animals and cell lines

A total of 32 Specific Pathogen-Free (SPF) adult male BALB/c mice weighing 18±4 g were purchased from Shanghai Slake Experimental Animal Co., Ltd. (Animal license number SCXK (Shanghai) 2017–0005), Animal ethics code: PZSHUTCM211227011. The mice were raised at the Experimental Animal Center of Shanghai University of Traditional Chinese Medicine under controlled conditions (temperature of 25 °C, relative humidity of 45 %, 12-h light-dark cycle) and provided with free access to food and water. The research was conducted in accordance with ethical standards, the Declaration of Helsinki and the related national and international guidelines. Human renal cortex proximal convoluted tubule epithelial cells (HK-2) were obtained from the cell bank of the Chinese Academy of Sciences.

2.3. Reagents and antibodies

Potassium oxoxazine (Shanghai Macklin Biochemical Technology Co., Ltd C10097951, P831461), monosodium urate (Sigma U2875-5G), polyvinylidene fluoride (Millipore, USA.
, IPVH00005), α-tubulin (ABclonal, China, AC012), p44/42MAPK(ERK1/2) (Cell Signaling Technology, 4695 S), p-p44/42MAPK (ERK1/2) (Cell Signaling Technology, 4370 S), caspase-3(Cell Signaling Technology, ab184787) , Bcl-2 (Cell Signaling Technology, 3498 S), Bax (Abcam, UK, ab182733), U0126–EtOH (Med Chem Express, USA, HY-12031), HRP labeled goat anti-mouse IgG, HRP labeled goat anti-rabbit IgG, Alexa Fluor 488 labeled goat anti-rabbit IgG, Alexa Fluor 647 labeled goat anti-mouse IgG (Shanghai Biyuntian Biotechnology Co., Ltd, A0216, A0208, A0423, A0473)

2.4. Experimental instruments

Biological tissue embedding machine, automatic tissue dehydration machine, drying machine, spreading machine, (KD-TS3A, KD-BMBL, KD-P, KD-H, Kedi Instrument Equipment Co., Ltd., Jinhua City, Zhejiang Province)、Fluorescent microscope (Nikon 80i, Japan), Transmission Electron Microscope (FEI, Tecna G2 BioTWIN, Germany), Protein electrophoresis tank (US, Bio-Rad, 165–8004), electrophoresis instrument and membrane transfer instrument (US, Bio-Rad, 165–8004), microplate reader (US, BioTek, Synergy 2), centrifuge (US, Beckman, Avanti J-E), gel imaging system (China, Shanghai Tianneng Technology Co., Ltd., Tanon-5200).

2.5. Solution preparation

The solubility of uric acid in water is 62.3 μ g/mL, and it is 25–50mg/mL in 1 M sodium hydroxide solution. Based on the characteristics of uric acid and literature reports, a 10mg/mL uric acid solution was prepared using 1 M sodium hydroxide (ultrasound-assisted dissolution). After no crystallization was observed under the microscope, the solution was filtered through a 0.22 μ m filter and stored in a refrigerator at 4 °C for future use.

Weigh an appropriate amount of SZF dry powder, dissolve it fully in DMSO through methods such as vortex and ultrasound, and prepare a solution of SZF dry powder with a concentration of 60 mg/mL, and store it at 4 °C for future use.

2.6. Component identification of SZF

Chromatographic conditions: Agilent ZORBAX RRHD SB-Aq (2.1 × 100 mm, 1.8 μ m); Mobile phase: acetonitrile (A) −0.1 % formic acid aqueous solution (B), gradient elution, as shown in Table 1, volume flow rate: 0.3 mL/min; Detection wavelength: 330 nm; Column temperature: 30 °C; Injection volume: 2 μL. Mass spectrum conditions: electrospray ionization (ESI) - positive/negative ion mode. See Table 2 for mass spectrum parameters.

Data collection and processing were carried out using Analyst TF 1.7.1 and Peakview 1.2 software, respectively. During identification, priority should be given to matching mass spectrometry data with the Natural Products HR-MS/MS Spectral Library 1.0 database. Compounds should be preliminarily screened based on the score information of each chromatographic peak, and further confirmed based on the primary and secondary information of each chromatographic peak. Compounds not included in the database are identified based on literature reports, mass spectrometry fragmentation patterns, etc.

2.7. Prediction of active ingredients and targets in SZF

Collect the active ingredients of *Plantago asiatica* L, *Sinapis alba*, *Vaccariae Semen*, *Semen malvae verticillatae* (Abutili Semen) through TCMSP, TCMID, ETCM, SwissTargetPredict, and BAT-MAN databases [13–16]. Active ingredients and their corresponding gene targets with an oral availability (OB value) of ≥30 % and a drug similarity (DL value) of ≥0.18 were selected as per the criteria. The target genes were standardized through the Uniprot and STRING platforms [17,18].

2.8. Identification of targets associated with hyperuricemia

Disease targets of hyperuricemia were collected from DisGeNET (https://www.disgenet.org/) and GeneCards (https://www.genecards.org/) databases [19,20]. The keywords “hyperuricemia" were used for the search, and the disease targets from both databases were merged to remove duplicates, resulting in the final set of disease targets for subsequent analysis.

2.9. Construction of drug component target disease interaction network and screening of key targets

The drug target genes and disease targets were imported into the Venny platform to obtain the common target genes shared by both drug targets and disease targets. These common target genes were used to construct a drug component target disease protein interaction (PPI) map using the STRING database (https://string-db.org) with a minimum interaction score of “moderate confidence (0.4)". The common genes were also introduced into Cytoscape 3.9.1 software to construct a component disease target network, and nodes with a degree value (DC) ≥ twice the median were selected to identify the core target network.

2.10. GO enrichment and KEGG pathway analysis

The common genes were imported into the DAVID database [21] for GO enrichment analysis and KEGG pathway analysis. The GO enrichment analysis included biological processes (BP), cellular components (CC), and molecular functions (MF), while KEGG pathway analysis helped identify important signaling pathways. The results of GO enrichment analysis and KEGG pathway analysis were

Table 1
Mobile phase gradient.

Time (min)	A%	B%
0 ~ 5	0	100
5 ~ 10	0 ~ 6	100 ~ 94
10 ~ 30	6 ~ 9	94 ~ 91
30 ~ 40	9 ~ 14	91 ~ 86
40 ~ 50	14 ~ 25	86 ~ 75
50 ~ 70	25 ~ 35	75 ~ 65
70 ~ 75	35 ~ 95	65 ~ 5
75 ~ 77	95	5
77 ~ 77.1	95 ~ 0	5 ~ 100
77.1 ~ 80	0	100

Table 2
Mass parameters (Sciex Triple TOF 4600 LC-MS).

MS parameters	Parameter value	MS/MS parameter	Parameter value
TOF mass range	50 ~ 1700	MS/MS mass range	50 ~ 1250
Ion Source Gas 1 (psi)	50	Declustering Potential (V)	100
Ion Source Gas 2 (psi)	50	Collision Energy (eV)	±40
Curtain Gas (psi)	35	Collision Energy Spread (eV)	20
Ion Spray Voltage Floating (V)	−4500/5000	Ion Release Delay (ms)	30
Ion Source Temperature (°C)	500	Ion Release Width (ms)	15
Declustering Potential (V)	100		
Collision Energy (eV)	10		

visualized and analyzed using the microbiological information platform.

2.11. Molecular docking

The core target CASP3 was selected for molecular docking with the active ingredients of the drug. The 3D structure file (in PDB format) corresponding to CASP3 was downloaded from the Protein Data Bank (https://www.rcsb.org) and prepared using Pymol software. The chemical structure of the active ingredient (in mol2 format) was obtained from TCMSP and prepared as a small molecule ligand. The docking box was adjusted to the appropriate size using Auto Dock Tools 4.2.6 software, and the docking parameters were set to perform semi-flexible docking on the dpf file using AutoDock. The binding energy was calculated, and the results were analyzed and visualized using Pymol software. When the binding energy is less than 0 (KJ/mol), it indicates that the ligand can spontaneously bind to the receptor, and when it is less than - 5 (KJ/mol), it indicates that it can dock stably.

2.12. Cell viability test

HK-2 cells were cultured in vitro and treatd with concentration gradients of 0, 50, 100, 150, 200, 250, 300, 350, 400, 450, and 500 μ g/mL Uric Acid, with 4 side wells set for each concentration gradient. The best concentration was selected to prepare the hyperuricemia cell model.

2.13. Cell culture and intervention

HK-2 cells were cultured in DMEM/F12 medium containing 10 % FBS and 1 % double antibody (penicillin-streptomycin), 37 °C, 5 % carbon dioxide incubator environment, and the solution was changed every 3 days. The cells were starved in 0.5 % FBS and 1 % penicillin-streptomycin DMEM/F12 culture medium for 24 h before intervention. Based on previous literature, ERK1/2 inhibitor (500 nM) is intervened 1 h in advance, and UA (200 mg/mL) and SZF (300μg/mL) are added to the corresponding six-well plate. After 24 h of dosing, the cells were scraped off and the protein content was quantified.

2.14. Western blot

Cell planking, after 24 h of medication intervention, add 100 μL RIPA lysate, after 30 min, the cells were scraped off and centrifuged at 4 °C at 12,000 r/min for 10 min. The remaining steps were the same as above. After membrane cutting, add the first antibody (*p*-ERK1/2, caspase-3, Bax: 1:2000; Bcl-2: 1:1000; α- Tubulin: 1:5000), 4 °C, incubated overnight in a shaking table, recovered the primary antibody, PBST washed (the same as before), added the secondary antibody HRP labeled goat anti-mouse IgG (1:1000), goat anti-rabbit IgG (1:1000) respectively according to the source of the primary antibody, incubated at room temperature in a shaking table for 1 h, recovered the secondary antibody, PBST washed (the same as before), drip ECL luminous solution, took photos with the automatic gel imaging system, and calculated the protein gray value with ImageJ 1.8.0 software.

2.15. Immunofluorescence detection

After climbing the cells, we added drug intervention. After 24 h of drug intervention, the supernatant of the cells in the six-well plate was first removed, and then PBS was used to clean the six-well plate. Each well was washed three times with 1 mL PBS, each time for 5 min 4 % paraformaldehyde was added to fix for 15 min, and PBS was washed three times. 0.5 % Triton perforation for 15 min, PBS cleaning three times. Seal with 1 % BSA for 40 min, add the first antibody (Bax, Bcl-2:1:200) diluted with 1 % BSA, and incubate at 4 °C overnight. Add fluorescent secondary antibody (1:500) to avoid light and incubate at room temperature for 60 min. DAPI staining for 5 min, place the circular slide on a glass slide and observe the results under a fluorescence microscope.

2.16. Annexin V-FITC/Propidium Iodide (PI) assay

The Annexin V-FITC/Propidium Iodide (PI) assay was used to detect apoptosis in cells from different groups. Approximately 1 × 10^5 cells were suspended in 100 μL of cell suspension, to which 5 μL of Annexin V and 10 μL of PI were added. The mixture was gently

mixed and then incubated at room temperature in the dark for 15 min. The apoptotic status of cells in each group was observed under a fluorescence microscope. Quantitative analysis was performed using Image J software.

2.17. Animal models and treatments

32 BALB/c mice were randomly divided into four groups: control group, model group, Febuxostat group, and SZF group, with 8 mice in each group. The control group was administered an equal amount of normal saline by gavage, while the other groups were given potassium oxoxazine (250 mg/kg) by gavage to induce hyperuricemia. After 4 h of modeling, the Febuxostat group received a dose of Febuxostat (6 mg/kg) by gavage, the SZF group received a dose of traditional Chinese medicine SZF (562.5 mg/kg) by gavage, and the control group and model group received an equal amount of normal saline by gavage for 2 weeks.

2.18. Sample collection

On the 13th day of the experiment, the mice fasted, and on the 14th day, the 24-h urine volume of the mice was collected. The mice were then anesthetized by intraperitoneal injection of 0.8 % pentobarbital sodium. One side of the renal cortex of the mouse kidney was quickly cut off (1 mm × 1 mm × 1 mm) and fixed in 2.5 % glutaraldehyde. The other side of the kidney was circumcised for pathological detection of renal tissue, and the remaining renal tissue was used for Western blot, immunohistochemistry, and other tests.

2.19. Renal pathology

The mouse kidney tissue was fixed with 90 % ethanol for 24 h and subjected to gradient ethanol dehydration, wax immersion, paraffin embedding, and slicing (thickness 3 μm). After dewaxing, the sections were stained using Hematoxylin and Eosin (HE), Periodic Acid-Schiff (PAS), and Masson staining techniques. The stained sections were then sealed with neutral resin for observation of the pathological morphology of mouse kidney tissue under light microscopy.

2.20. Immunohistochemistry

The paraffin sections of kidney tissue were dewaxed, subjected to antigen retrieval, and sealed at room temperature for 30 min with 3 % BSA. The first antibodies against Bax (dilution ratio: 1:50) and Bcl-2 (dilution ratio: 1:50) were diluted and incubated overnight at 4 °C. The sections were then washed with phosphate-buffered saline with Tween 20 (PBST) and incubated at room temperature for 1 h with the appropriate secondary antibody. DAB staining was performed to visualize the expression of Bax and Bcl-2, and the sections were sealed with neutral resin. Under light microscopy, positive expression of Bax and Bcl-2 was observed as brown and yellow particles, respectively.

2.21. Western blot

A total of 20 mg of kidney tissue was collected and 100 μl of RIPA lysis solution was added. The tissue was placed in a homogenizer and ground for 1 min to prepare tissue homogenate. The homogenate was then subjected to centrifugation at 4 °C at 13,000 rpm for 10 min. The protein-containing supernatant was collected for further analysis using Western blot, following the same steps as described earlier.

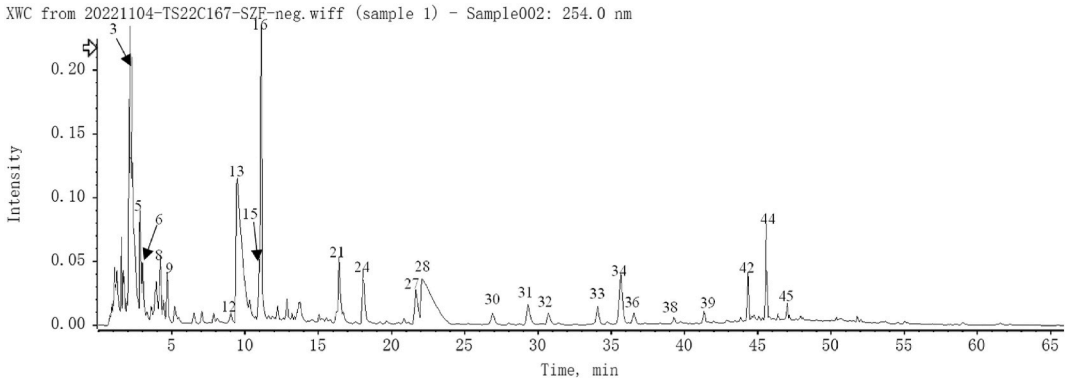

Fig. 1. UPLC UV Chromatogram of SZF Compound Sample −254 nm.

Table 3
Active ingredients and sources of SZF.

Table 3. Active ingredients and sources of SZF		
No.	Active ingredients	sources
1(CQ1)	(4aS,6aR,6aS,6bR,8aR,10R,12aR,14bS)-10-hydroxy-2,2,6a,6b,9,9,12a-heptamethyl-1,3,4,5,6,6a,7,8,8a,10,11,12,13,14b-tetradecahydropicene-4a-carboxylic acid	*Plantago asiatica L*
	Dinatin	
2(CQ2)	sitosterol	
3(CQ3)	daucostero_qt	
4(CQ4)	Dihydrotricetin	
5(CQ5)	Hypolaetin	
6(CQ6)	orobanchoside_qt	
7(CQ7)	plantaginin_qt	
8(CQ9)	quercetin	
9(A1)	6-Hydroxyluteolin	
10(CQ10)	Plantagoside	
11(CQ12)	Stigmasterol	
12(B1)	Uniflex BYO	
13(BJ1)	2-(2-phenylethyl)-6-[[(5S,6R,7R,8S)-5,6,7-trihydroxy-4-keto-2-(2-phenylethyl)-5,6,7,8-tetrahydrochromen-8-yl]oxy]chromone	*Sinapis alba*
14(BJ2)	Sinoacutine	
	Formononetin	
15(BJ3)	Isorhamnetin	
16(BJ4)	Kaempferol	
17(BJ5)	Luteolin	
18(BJ6)	Maackiain	
19(BJ7)	Pinocembrin	
20(BJ8)	Sakuranetin	
21(BJ9)	3'-Methoxydaidzein	
22(BJ10)		
23(BJ11)		
24(BJ12)	(-)-Catechin	
25(BJ13)	Calycosin	
26(BJ14)	Catechin	
27(BJ15)	Cianidanol	
28(B1)	Stigmasterol	*Vaccariae Semen*
29(LX2)	Isovitexin	
30(LX3)	(3S,6S,9S,12S)-6-(1H-indol-3-ylmethyl)-12-isopropyl-3,9-dimethyl-1,4,7,10,13-pentazacyclopentadecane-2,5,8,11,14-pentone	
	Quercetin	
31(A1)	Sucrose	
32(DK1)	Amylum	*Semen malvae verticillatae*
33(DK2)	Linoleic Acid	
34(DK3)		

2.22. Statistical analysis

The experimental results were statistically processed using SPSS 25.0 and GraphPad Prism 8.0 software. The data is expressed in -x ± s and the variance between groups is homogeneous. Those who obey the normal distribution are tested with parameters, while those who do not obey the normal distribution and have uneven variance are tested with non-parameters. The difference with $P < 0.05$ is statistically significant.

3. Results

3.1. Quality control and component identification of SZF

The analysis of UPLC-Q-TOF-MS (Fig. 1) identified a total of 49 components in SZF freeze-dried powder.

3.2. 3.2prediction of active ingredients and targets of drugs in SZF

Total of 34 active ingredients of SZF were selected and listed in Table 3. Using these active ingredients, 1277 drug action targets were screened, and after removing duplicates and standardizing them to gene symbols through the UniProt database, a total of 597 action targets were obtained.

3.3. Collection of targets associated with hyperuricemia and common gene identification

By searching the disease name “hyperuricemia" in the DisGeNET and GeneCards databases, 1019 disease targets were retrieved. After removing duplicates, there were 890 remaining disease targets. Intersecting these disease targets with the action targets of SZF components resulted in 99 common targets. Fig. 2 (A-B) illustrates the intersection of SZF components and their various drugs with the disease targets.

3.4. PPI network construction and core target screening

The common targets were imported into STRING to construct a Protein-Protein Interaction (PPI) network, resulting in 1400 edges (interaction relationships) and 99 nodes, with an average node degree value of 28.3 (see Fig. 3). Additionally, the drugs, active ingredients, and disease targets were imported into Cytoscape to construct a drug-active ingredient-disease target network (Fig. 4). Based on the condition of degree value (DC) $\geq$ 2 times the median, 12 key targets were selected through Cytoscape. The screening process and results are presented in Figs. 5–7.

3.5. GO enrichment analysis

To further investigate the mechanisms underlying SZF’s efficacy in treating HUA, we conducted GO enrichment analysis on the 99

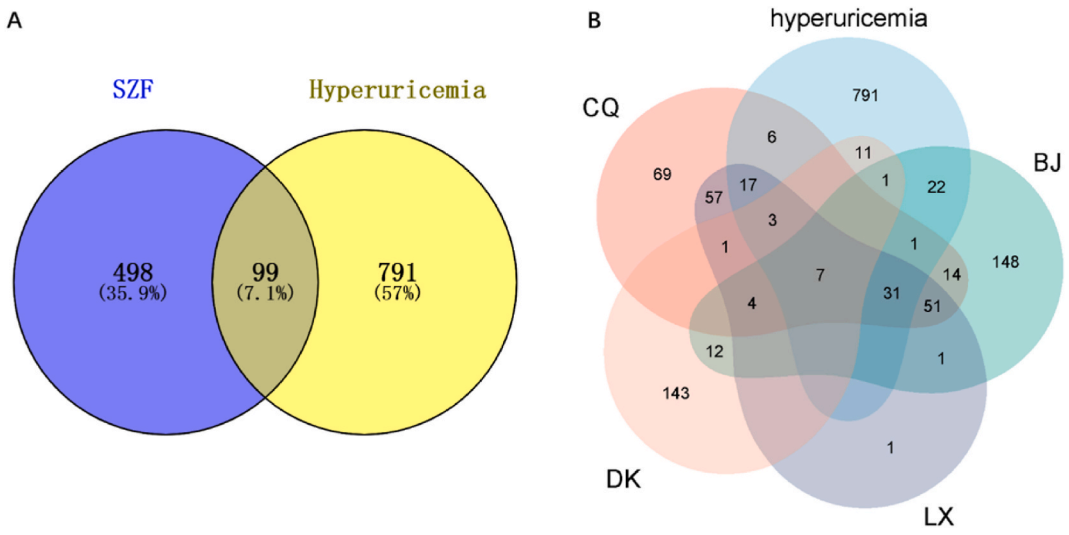

Fig. 2. A: Intersection of all active components of SZF with corresponding targets and diseases. B: Intersection between the corresponding targets of SZF drugs and diseases.
SZF : shizihfang Decoction **CQ:** *Plantago asiatica* L **BJ:** *Sinapis alba* **LX:** *Vaccariae Semen* **DK:** *Semen malvae verticillatae*.

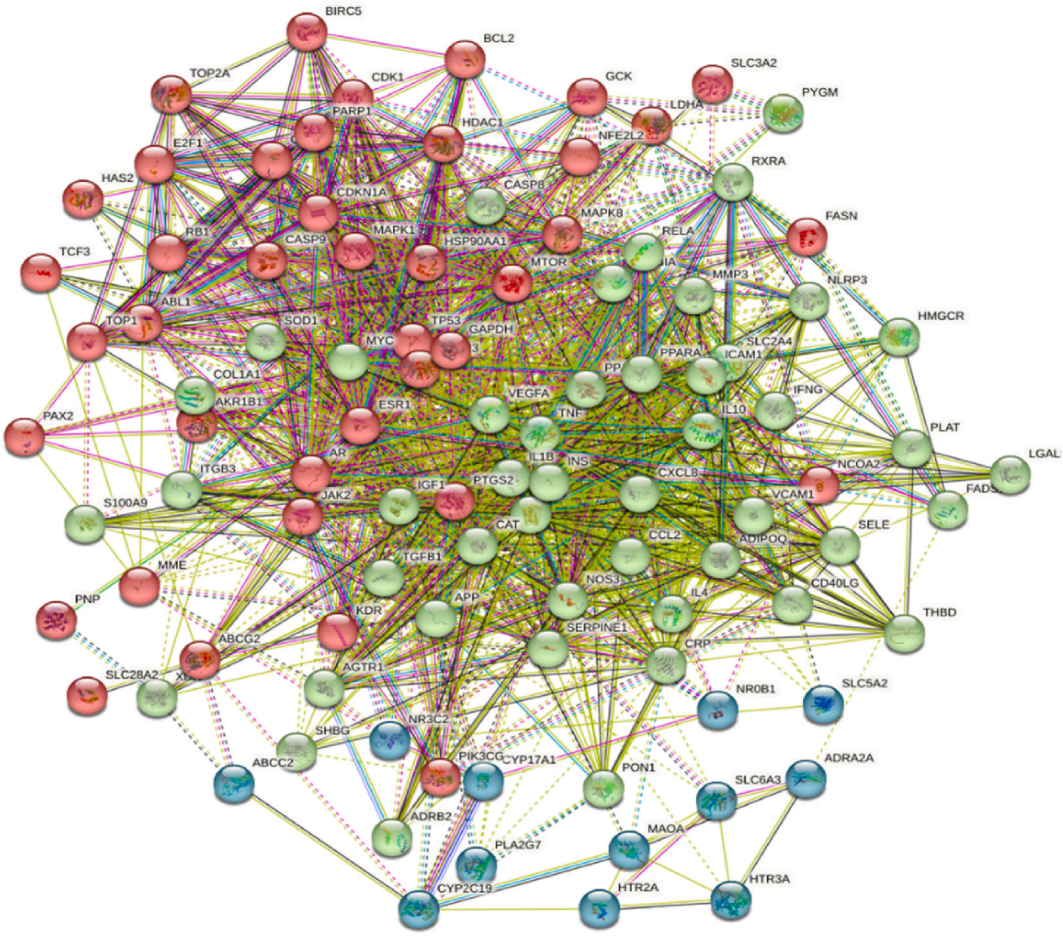

Fig. 3. PPI network diagram of drug composition target disease common target.

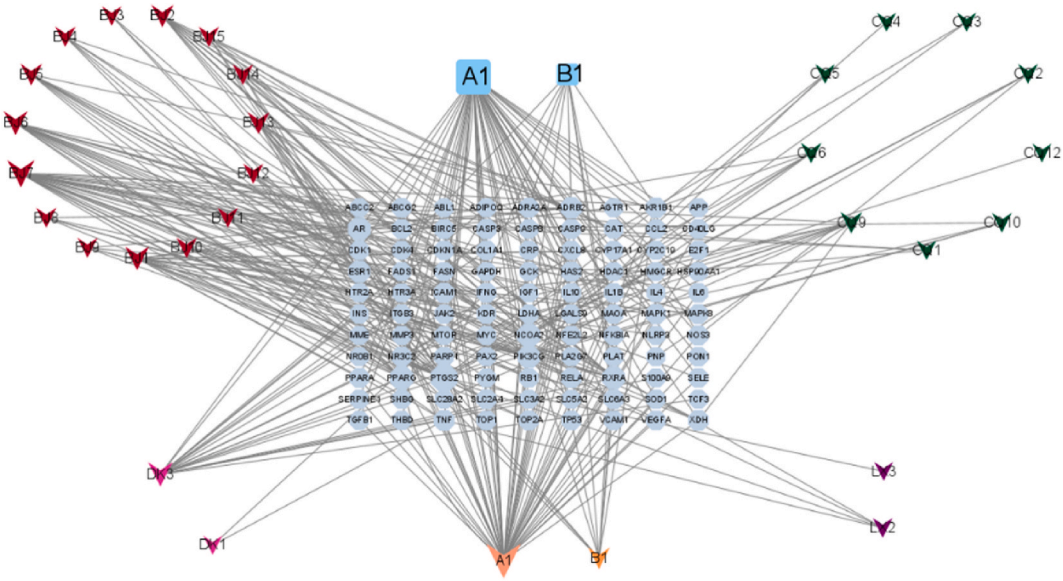

Fig. 4. Active ingredient disease target network.

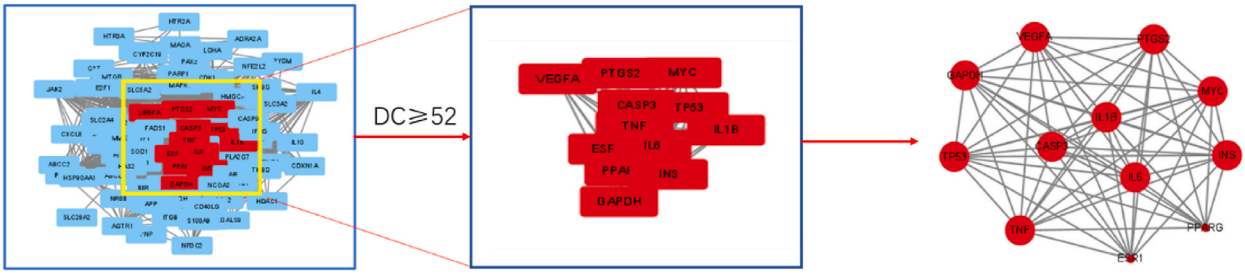

Fig. 5. Screening process of key drug targets.

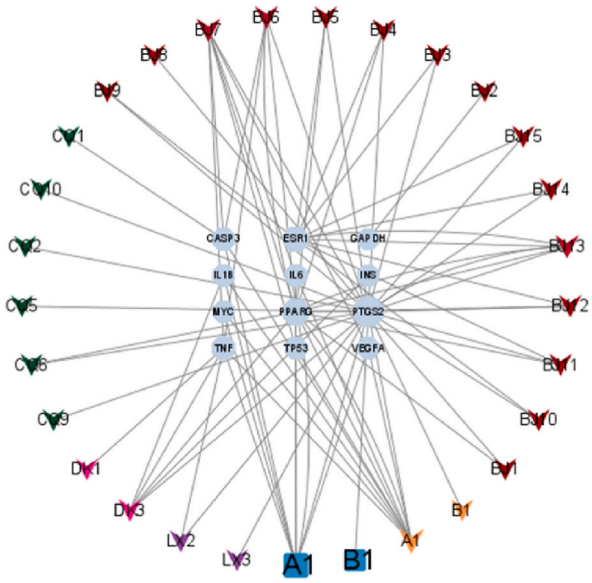

Fig. 6. Active ingredient key target network.

common targets (corrected for $P < 0.05$ as the significance level). The analysis revealed 354 enriched projects, including 270 biological processes (BP), 46 molecular functions (MF), and 32 cellular components (CC). The top 30 enriched terms for BP, MF, and CC are depicted in bubble charts (Fig. 7). The highly enriched BP terms involve various processes, such as positive and negative regulation of gene expression, inflammatory response, positive and negative regulation of cell apoptosis, positive regulation of ERK1 and ERK2 cascades, and positive regulation of protein phosphorylation. As for MF terms, protein binding, enzyme binding, transcription factor binding, and protein binding were highly enriched. Additionally, CC terms included cytoplasm, nucleus, mitochondria, and extracellular vesicles.

3.6. KEGG pathway analysis

We performed KEGG pathway enrichment analysis on the 99 common targets (corrected $P < 0.05$ as the significance level). Among the 126 highly enriched pathways, we selected the top 50 pathways, which are represented in a sankey + dot plot (Fig. 8). These pathways encompass various signaling pathways, such as Pathways in Cancer, Lipid and Atherosclerosis, AGE-RAGE signaling pathway in diabetic complications, PI3K-Akt signaling pathway, IL-17 signaling pathway, TNF signaling pathway, HIF-1 signaling pathway, NOD-like receptor signaling pathway, MAPK signaling pathway, Apoptosis, and others.

Based on the results of GO and KEGG analyses, it is evident that SZF may exert its therapeutic effects on HUA by engaging in cascade reactions related to cell apoptosis, regulating the ERK1/2 and MAPK signaling pathways, and targeting apoptosis-related pathways. The ERK1/2 signaling pathway, being a branch of the MAPK signaling pathway, is closely linked to the cancer-related pathway, which was also highly enriched in the KEGG analysis. Previous research has consistently shown a strong connection between the ERK1/2 signaling pathway and apoptosis [22–26]. The significant targets identified by the protein action network are closely associated with apoptosis and inflammation, with caspase-3 playing a pivotal role in cell apoptosis, affecting both internal and external apoptosis pathways. Consequently, we plan to validate these findings through molecular docking analysis, in vitro experiments, and in vivo studies to strengthen the reliability of our network pharmacology results.

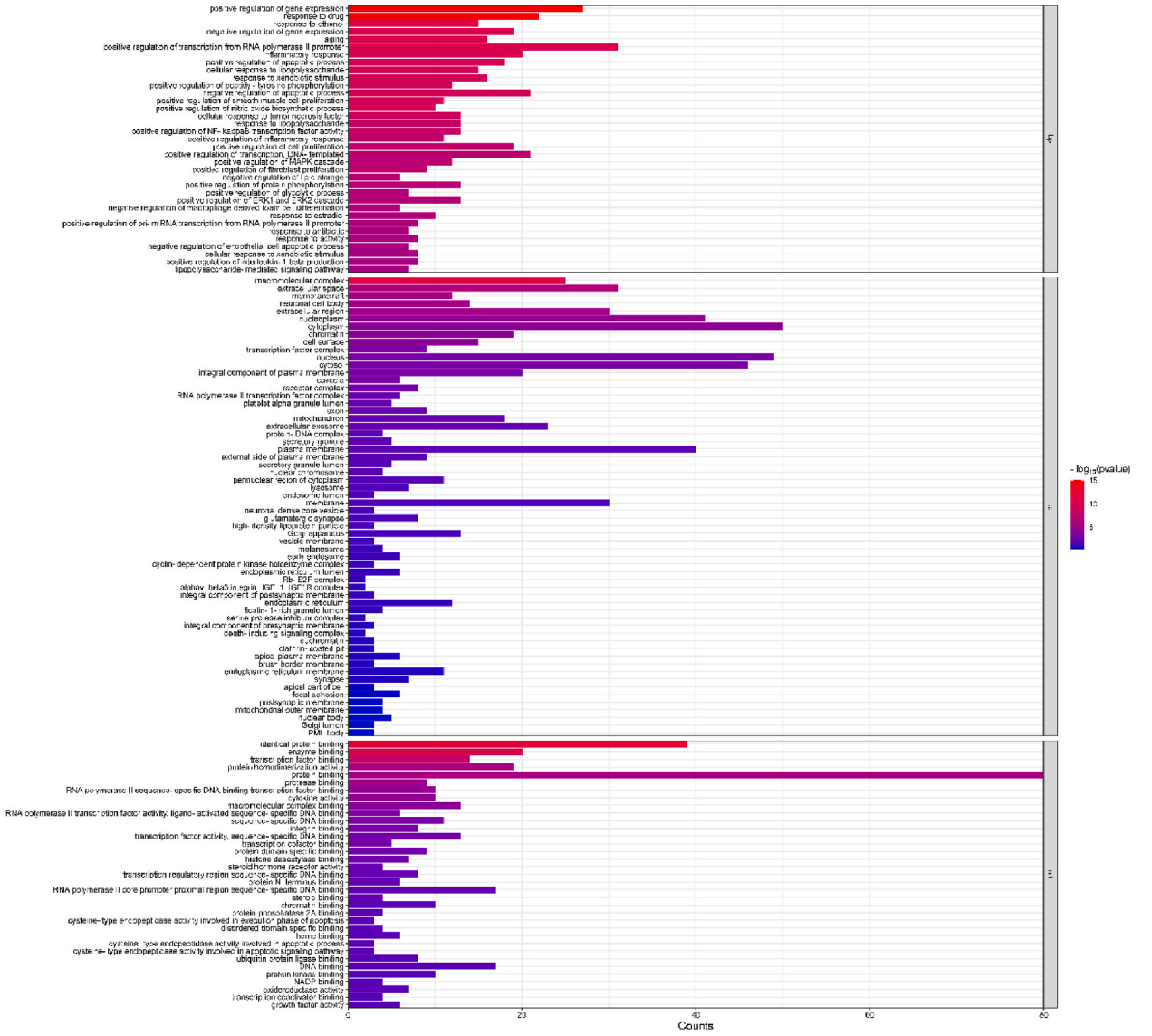

Fig. 7. Go BP、MF、CC enrichment bubble chart.

3.7. Molecular docking

The active ingredients of SZF were docked with the core protein CASP3, and the results are presented in Table 4. Among the active ingredients, quercetin, luteolin, and kaempferol formed stable docking with CASP3, with their binding energies lower than −5.0 kJ/mol. However, (4aS, 6Ar, 6bR, 8aR, 10 R, 12aR, 14bS) - 10-hydroxy-2,2,6a, 6 b, 9,9,12a-heptamethyl-1,3,4,5,6,6a, 7,8,8a, 10, 11, 12,13,14 b-tetradecahydropicene-4a-carboxylic acid showed the highest binding energy, but it did not form a hydrogen bond with the residue. Consequently, quercetin exhibited the best binding to the core protein CASP3 (Figs 9-10).

3.8. In vitro experiment

3.8.1. Effects of different uric acid concentrations on cell activity

The results show that in Fig. 11 when the uric acid concentration is between 0 and 300μg/mL, the effect on cell activity is relatively small. When the uric acid concentration exceeds 350ug/mL, there is a statistically significant difference compared to the control group ($p < 0.05$), and cell activity is inversely proportional to the uric acid concentration.

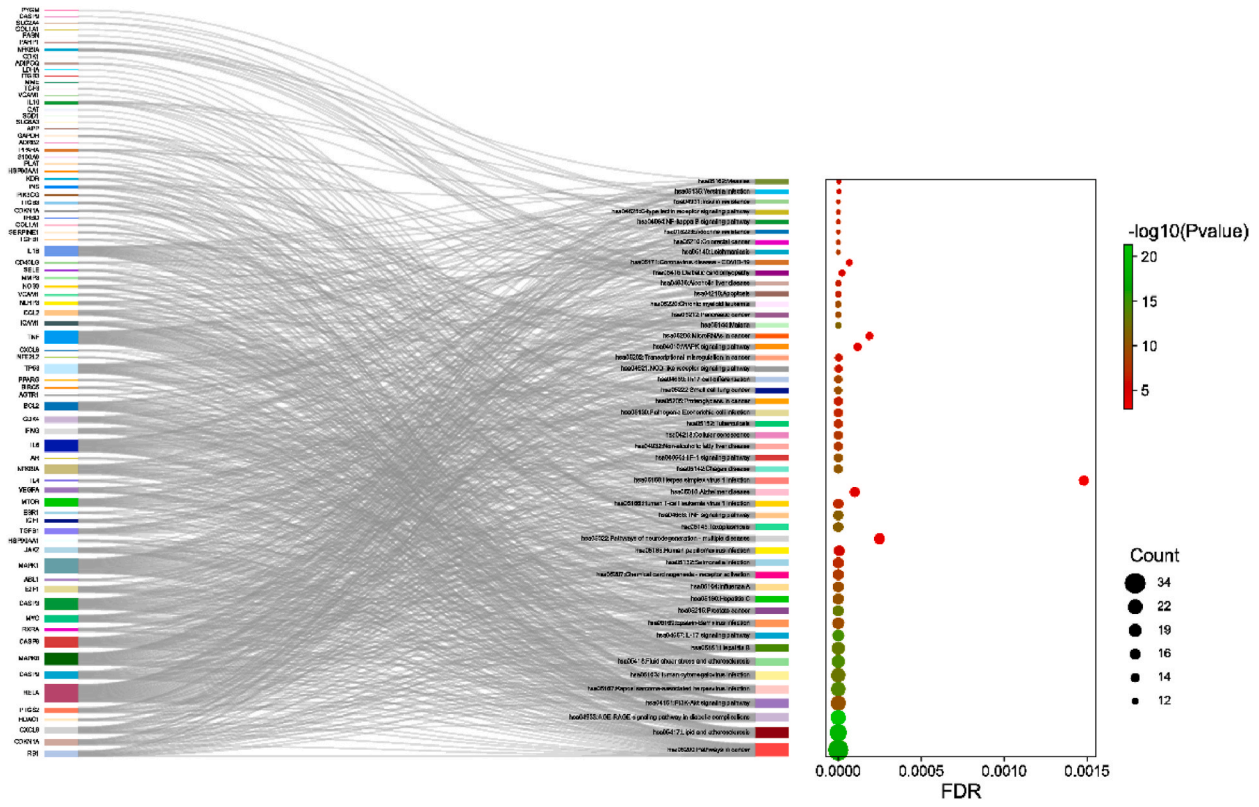

Fig. 8. KEGG pathway analysis diagram.

Table 4
Molecular docking results.

Ligand component	Receptor protein	PDB ID	Binding energy (kJ/mol)
Quercetin	CASP3	3kjf	−15.40
Luteolin	CASP3	3kjf	−13.64
Kaempferol	CASP3	3kjf	−9.50
(4aS , 6Ar,6 bR,8aR,10R,12aR,14bS) -10-hydroxy-2,2,6a,6 b,9,9,12a-heptamethyl-1,3,4,5,6,6a,7,8,8a,10,11,12,13,14 b-tetradecahydropicene-4a-carboxylic acid	CASP3	3kjf	−20.84

3.8.2. Effects of uric acid and SZF on the expression of p-ERK1/2, ERK1/2, Caspase-3, Bax, and Bcl-2 proteins in human renal tubular epithelial cells

In HK-2 cells, the expression of *p*-ERK1/2 and caspase-3 proteins increased in the model group compared to the control group ($P < 0.05$, $P < 0.05$), indicating a statistically significant difference. However, the expression of ERK1/2 protein remained unchanged ($P > 0.05$), showing no statistically significant difference. In the SZF group, inhibitor group, and model plus inhibitor group, the protein expression of *p*-ERK1/2 ($P < 0.01$, $P < 0.05$, $P < 0.05$) and caspase-3 ($P < 0.001$, $P < 0.001$, $P < 0.0001$) decreased compared to the model group, with a statistically significant difference. The ERK1/2 protein expression in the SZF group remained unchanged ($P > 0.05$), indicating no statistically significant difference. However, the ERK1/2 protein expression in the inhibitor group and model plus inhibitor group decreased ($P < 0.01$, $P < 0.05$), demonstrating statistically significant differences (Fig. 12 and Table 5).

3.8.3. Effects of uric acid and SZF on the expression of apoptosis-related proteins in HK-2 cells

In vitro immunofluorescence staining showed that compared with the control group, the expression of Bax in HK-2 cells in the model group increased; Compared with the model group, the expression of Bax in the inhibitor group, SZF group, and model plus inhibitor group decreased, as shown in Figs. 13 and 14, and Table 6.

3.8.4. The effects of SZF and uric acid on early and late apoptosis of HK2

The results of the Annexin V-FITC/PI assay showed that compared to the normal group, both early and late apoptosis were significantly increased in the model group. However, apoptosis was reduced in the inhibitor group, SZF group, and model plus

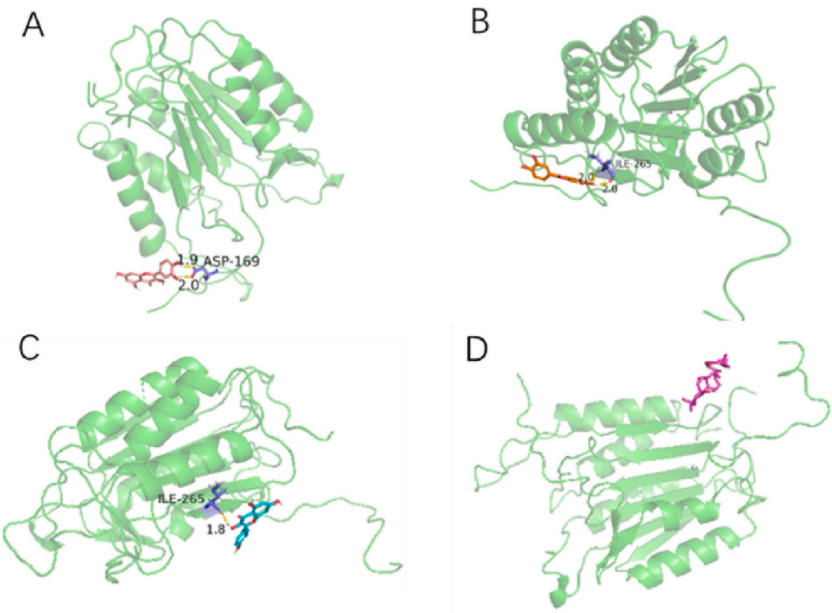

Fig. 9. Docking of active ingredients with CASP3 protein
A:Quercetin **B:**Luteolin **C:**kaemferol **D:** (4aS , 6Ar,6 bR,8aR,10R,12aR,14bS) -10-hydroxy-2,2,6a,6 b,9,9,12a-heptamethyl-1,3,4,5,6,6a,7,8,8a,10, 11, 12,13,14 b-tetradecahydropicene-4a-carboxylic acid.

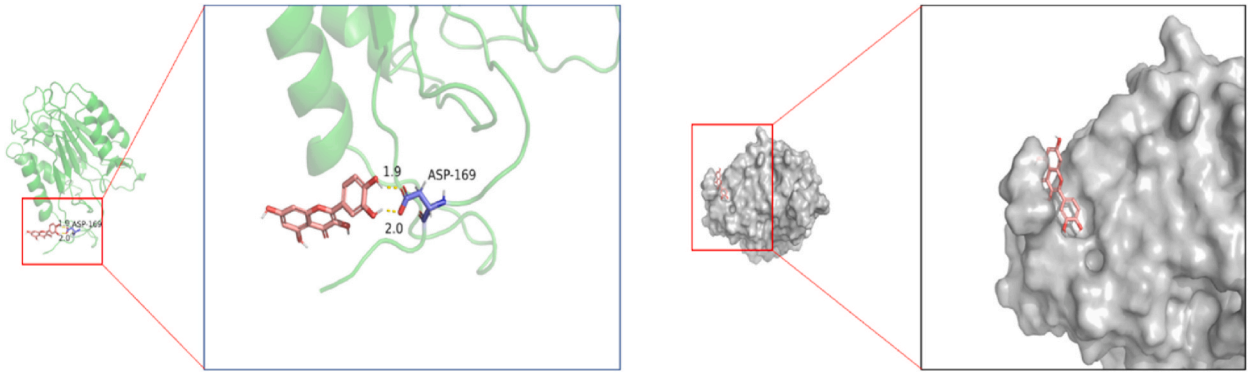

Fig. 10. The three-dimensional spatial structure and surface structure docking diagram of quercetin and casp3 protein.

inhibitor group compared to the model group, as shown in Figs. 15 and 16, and Table 7.

3.9. In vivo experiments

3.9.1. The effect of uric acid and SZF on pathological changes of kidney tissue in mice

Transmission electron microscopy revealed that the tubular epithelial cells in the control group of mice displayed a normal morphology with clear structure, no nuclear pyknosis, and no mitochondrial swelling. In contrast, renal tubular epithelial cells in the model group exhibited signs of apoptosis, such as chromatin edge agglutination, nuclear concentration, and slight swelling of mitochondria. However, the cell structure in the Febuxostat group and SZF group appeared normal (Fig. 17).

HE staining (Fig. 18) demonstrated that the model group mice exhibited disordered arrangement of renal tubules, slight lumen dilation, and infiltration of interstitial inflammatory cells compared to the control group. However, these pathological changes were alleviated in the SZF group and Febuxostat group compared to the model group. Masson staining (Figs. 19 and 20, Table 8) indicated that the model group showed slight fibrosis in the renal tubulointerstitium compared to the control group ($P < 0.0001$). However, renal tubulointerstitial fibrosis was reduced in the SZF group and Febuxostat group compared to the model group ($P < 0.0001$). PAS staining (Fig. 21) revealed infiltration of inflammatory cells in the renal tubulointerstitial tissue of the model group, which was alleviated in the SZF and Febuxostat groups compared to the model group.

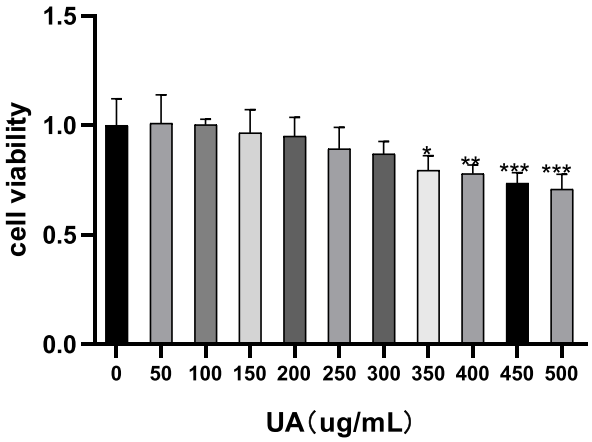

Fig. 11. Cell viability test.

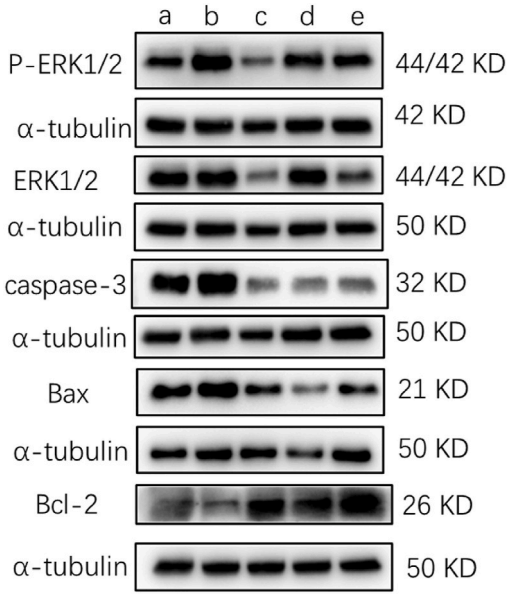

Fig. 12. Expression of *p*-ERK1/2, ERK1/2, caspase-3, Bax and Bcl-2 proteins in human renal tubular epithelial cells (HK-2)
a: Control b: Model c: Inhibitor d: SZF e: Inhibitor + Model.

Table 5
Expression of *p*-ERK1/2, ERK1/2, caspase-3, Bax and Bcl-2 proteins in human renal tubular epithelial cells ($\bar{x} \pm s$, $n = 4$)

Group	Quantity	*p*-ERK1/2	ERK1/2	Caspase-3	Bax	Bcl-2
Control	4	0.72 ± 0.12	1.08 ± 0.14	0.84 ± 0.05	0.83 ± 0.18	0.88 ± 0.16
Model	4	1.09 ± 0.13$^{\#}$	1.00 ± 0.10	1.08 ± 0.14$^{\#}$	1.10 ± 0.11$^{\#}$	0.59 ± 0.11$^{\#\#}$
Inhibitor	4	0.70 ± 0.20*	0.54 ± 0.12**	0.64 ± 0.16***	0.83 ± 0.18*	0.92 ± 0.13***
SZF	4	0.63 ± 0.23**	1.03 ± 0.09	0.64 ± 0.19***	0.51 ± 0.28****	1.02 ± 0.18****
Inhibitor + Model	4	0.72 ± 0.28*	0.58 ± 0.26**	0.53 ± 0.13****	0.67 ± 0.30***	0.87 ± 0.17**

Compared with the control group，$^{\#}$P < 0.05，$^{\#\#}$P < 0.01; compared with the model group，*P < 0.05 **P < 0.01，***P < 0.001，****P < 0.0001.

3.9.2. Positive expression of apoptosis-related proteins Bcl-2 and Bax in tissues

Immunohistochemistry showed that the expression of Bcl-2 in the kidney tissue of the model group mice decreased, while the expression of Bax increased compared to the control group. However, the SZF and Febuxostat groups exhibited an increase in Bcl-2 expression and a decrease in Bax protein expression in the kidney tissue of mice (Figs. 22–24, Table 9).

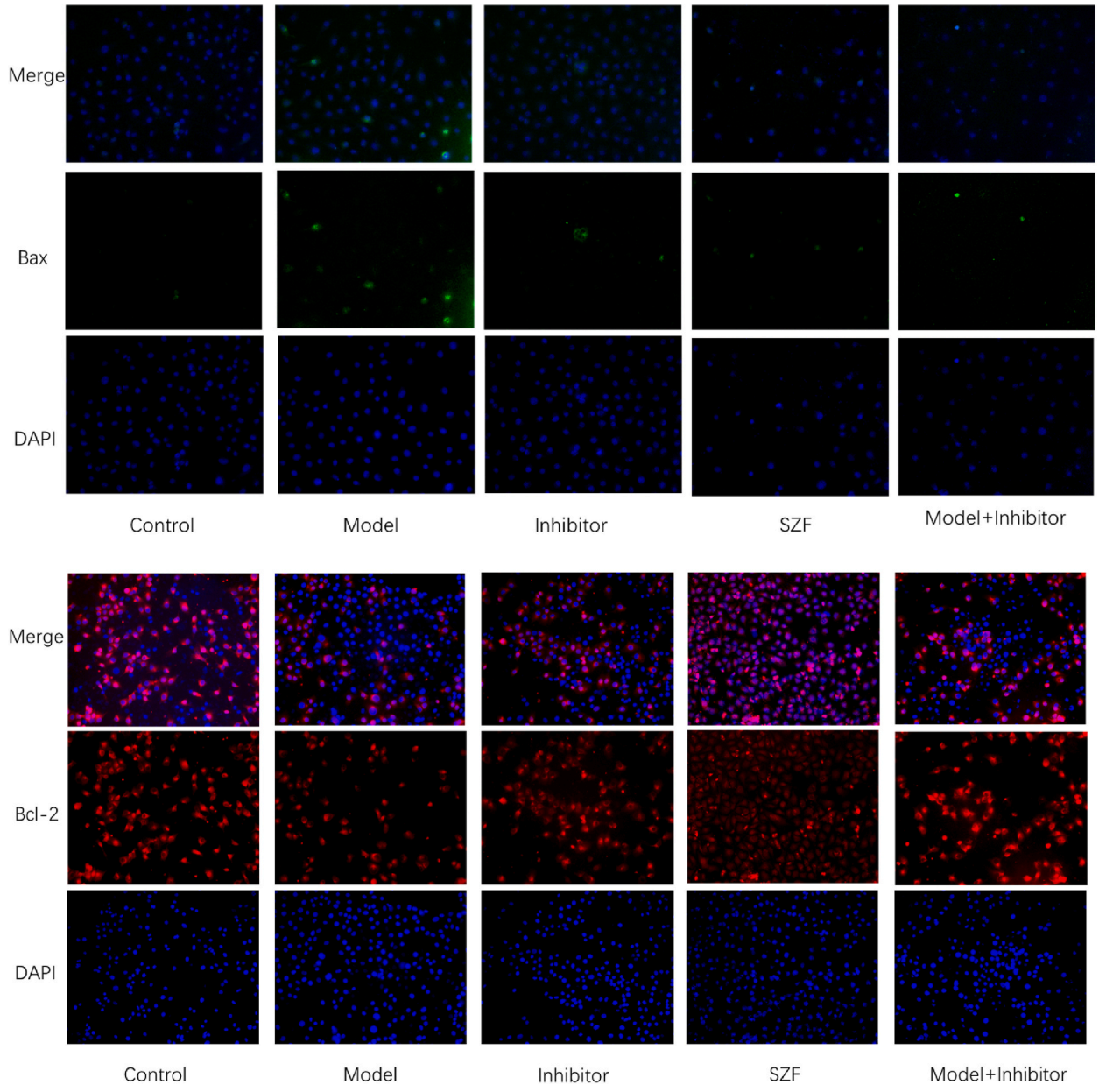

Fig. 13. Positive expression of Bax and Bcl-2 protein in HK-2 cells (IF， single label staining， × 200) .

3.9.3. The effect of SZF on the Expression of Bax and Bcl-2 proteins in mouse kidney tissue

In comparison to the control group, the expression of Bax protein in the kidney tissue of the model group mice increased ($P < 0.01$), while the expression of Bcl-2 protein decreased ($P < 0.01$). However, the expression of Bax protein in the kidney tissue of the SZF group and Febuxostat group mice decreased ($P < 0.001$), while the expression of Bcl-2 protein increased ($P < 0.001$), with statistically significant differences observed (Fig. 25, Table 10).

4. Discussion

According to the results of network pharmacology analysis, we determined that caspase-3 plays an important role in SZF Decoction in the treatment of hyperuricemia, and is closely related to biological processes such as ERK1/2 cascade reaction. The blood uric acid in hyperuricemia exceeds the normal level, leading to pathological changes such as inflammation, oxidative stress, and apoptosis in the kidney. Apoptosis is an important factor that causes damage to renal tubular epithelial cells. Studies have shown that the active apoptotic pathways in the glomerulus and tubular epithelium include survival factor deprivation-induced death, death receptor

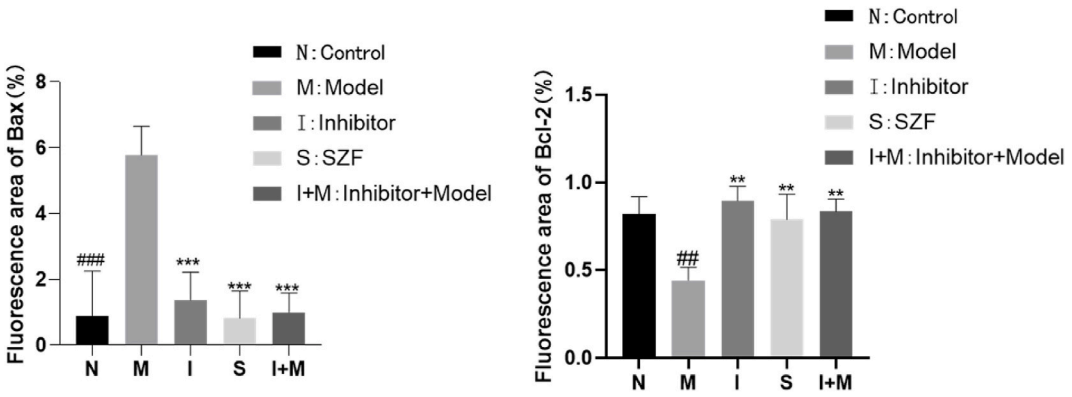

Fig. 14. Quantitative results of IF.

Table 6
Expression of Bax and Bcl-2 in HK-2 cells (% , $\bar{x} \pm s$, $n = 3$) .

Group	Quantity	Bax	Bcl-2
Control	3	0.89 ± 1.36	0.82 ± 0.10
Model	3	5.78 ± 0.88$^{\#\#\#}$	0.44 ± 0.07$^{\#\#}$
Inhibitor	3	1.37 ± 0.85***	0.90 ± 0.08**
SZF	3	0.82 ± 0.83***	0.80 ± 0.14**
Inhibitor + Model	3	1.01 ± 0.58***	0.83 ± 0.07**

Compared with the control, $^{\#}P < 0.05$, $^{\#\#\#}P < 0.001$, compared with the model, $^{*}P < 0.05$ $^{**}P < 0.01$, $^{***}P < 0.001$.

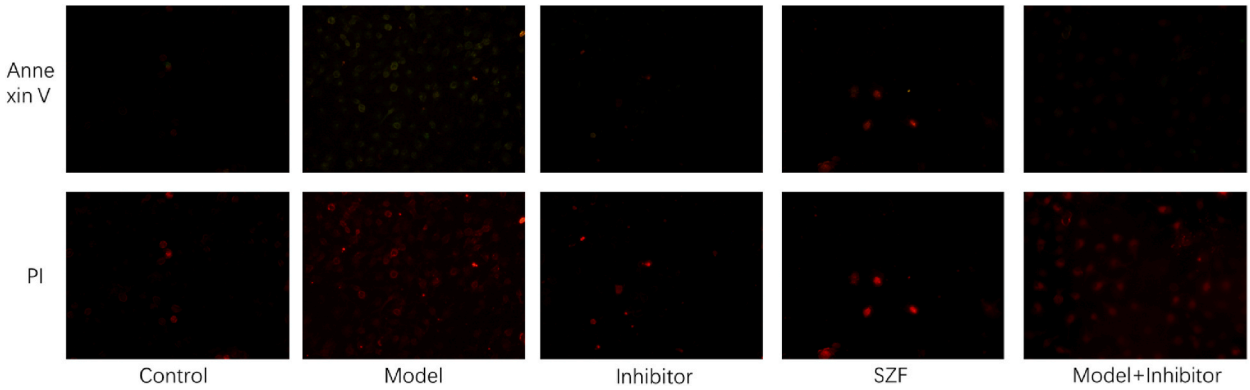

Fig. 15. Early and late apoptosis of HK2 cells in different groups.

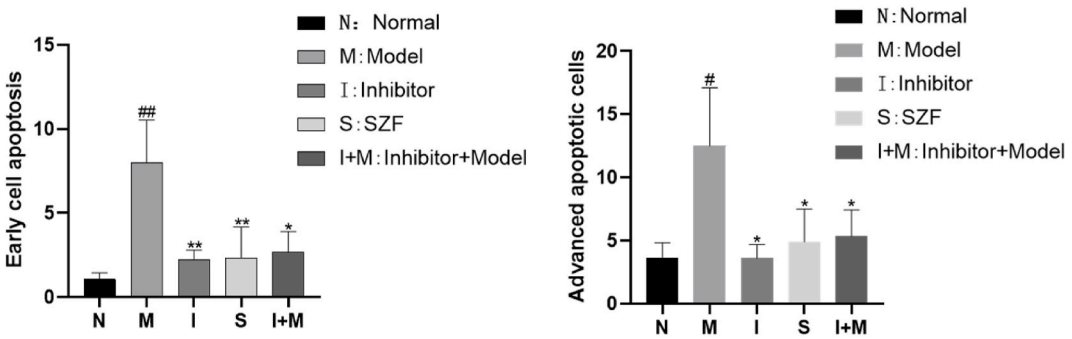

Fig. 16. Quantitative results of Annexin V-FITC/PI.

Table 7
Cell apoptosis in each group (% , $\bar{x} \pm s$, $n = 3$) .

Group	Quantity	Annexin V	PI
Control	3	1.05 ± 0.39	3.62 ± 1.23
Model	3	7.99 ± 2.56$^{\#\#}$	12.5 ± 4.61$^{\#}$
Inhibitor	3	2.24 ± 0.56**	3.60 ± 1.09*
SZF	3	2.35 ± 1.83.**	4.9 ± 2.61*
Inhibitor + Model	3	2.71 ± 1.20*	5.34 ± 2.10*

Compared with the control, $^{\#}P < 0.05$, $^{\#\#}P < 0.01$; compared with the model, $^{*}P < 0.05$, $^{**}P < 0.01$, $^{***}P < 0.001$, $^{****}P < 0.0001$.

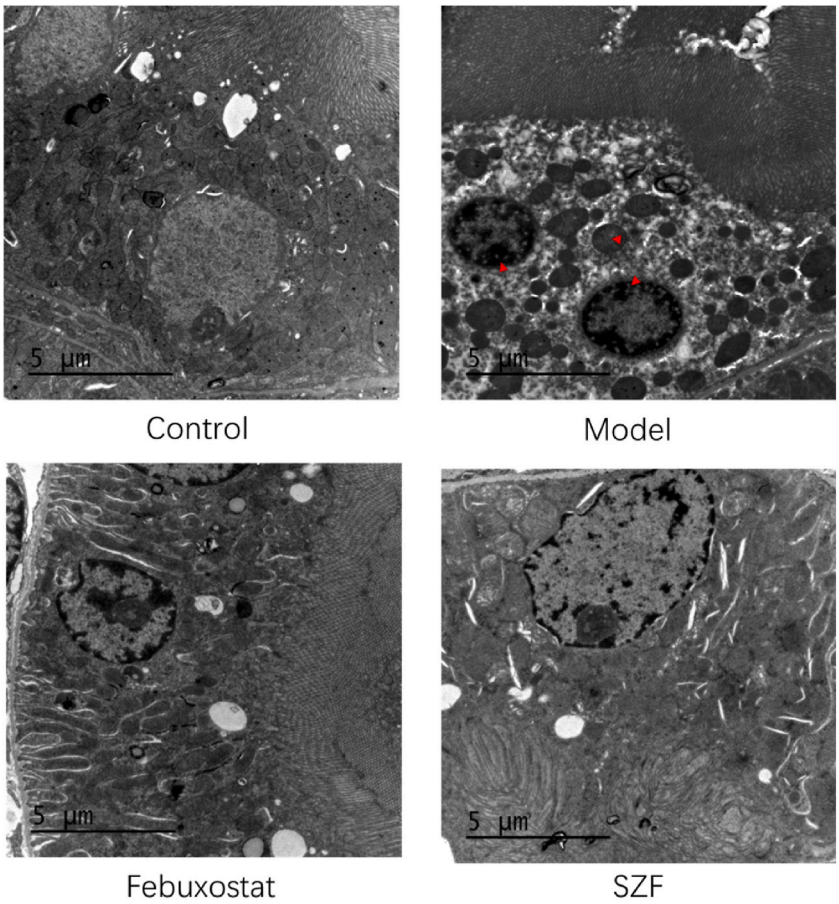

Fig. 17. Ultrastructure of Mouse Kidney Tissue (TEM × 4200). In the control group, renal tubular epithelial cells exhibited normal morphology with clear structural features, no nuclear condensation, and mitochondria evenly distributed around the cell nuclei. In the model group, chromatin exhibited peripheral aggregation, nuclear condensation, reduced mitochondrial quantity, mitochondrial swelling, and disorganized mitochondrial cristae (indicated by red triangles). In the Febuxostat group and SZF group, nuclear morphology tended toward normalcy, mitochondria showed mild swelling, and mitochondrial cristae exhibited clear alignment.

activation, mitochondrial damage, endoplasmic reticulum stress, lysosomal instability, and caspase cascade activation [27]. Caspase-3 and other caspase family-related members play a core role in the process of renal tubular cell apoptosis [28]. ERK1/2 signaling pathway is associated with hyperuricemia-related renal fibrosis and renal proximal tubule apoptosis. Studies have shown that the administration of selective inhibitor U0126 of ERK1/2 can reduce the progression of hyperuricemia-induced renal injury [29–31]. The molecular docking results indicate that multiple active ingredients in SZF decoction can form stable docking with CSAP3 protein, and the active ingredient quercetin forms the best binding with CASP3 protein.

Regarding the chemical composition analysis of Nanocnide lobata extract, it suggests the presence of flavonoids, which are potential chemical constituents and the basis for the clinical efficacy of herbal medicine [32]**. Quercetin, a widely occurring flavonoid compound in traditional Chinese medicine, is likely a key component of the SZF decoction.** Based on the above reasons, we chose the ERK1/2 signaling pathway and caspase-3-related cell apoptosis for further experimental verification. In vitro and in vivo experimental results showed that compared with the control group, the ERK1/2 signaling pathway in the model group

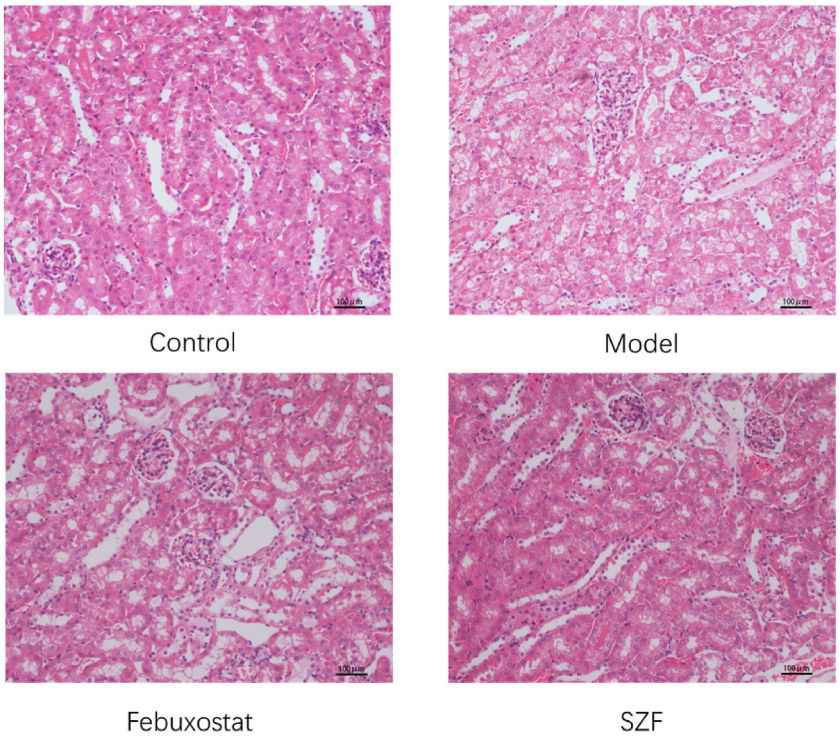

Fig. 18. Histomorphology of the Kidney (HE, × 200). In the control group, renal tubular epithelial cells displayed oval shapes with regular alignment, and no luminal dilation was observed. In the model group, renal tubular epithelial cells showed disorganized arrangement, epithelial cell shedding, vacuolar degeneration, luminal dilation, and interstitial infiltration of inflammatory cells. The non-Febuxostat group and Shizhi Fang group exhibited alleviation of the aforementioned changes.

was overactivated, and the expression of caspase-3 and apoptosis-related proteins was increased in the model group. Inhibiting the expression of this signaling pathway can reverse the above protein expression.

However, this study only provided preliminary evidence that Shizhi Fang attenuates kidney damage caused by hyperuricemia by inhibiting apoptosis in renal tubular epithelial cells, and the mechanism may be related to the ERK1/2 signaling pathway. Furthermore, the specific expression of upstream and downstream proteins in this pathway during the process has not been validated, and molecular docking only theoretically verified the active components' role in Shizhi Fang. Further experiments are required to confirm the effective components of Shizhi Fang in exerting its therapeutic effects. Additionally, this study did not investigate whether Shizhi Fang can reduce uric acid levels or its effect on uric acid-related transport proteins. The focus of this study was on the protective effect of Shizhi Fang on kidney damage caused by hyperuricemia, which is its unique contribution. In the future, further research is needed to address the limitations mentioned above.

5. Conclusion

In conclusion, the ERK1/2 signaling pathway is closely related to the apoptosis of renal tubular epithelial cells induced by hyperuricemia. SZF decoction reverses the high expression of caspase-3 and apoptosis-related proteins in hyperuricemia and plays a role in treating hyperuricemia, which is achieved by inhibiting the expression of the ERK1/2 signaling pathway. This study provides a preliminary theoretical basis and experimental basis for the mechanism of SZF decoction in treating hyperuricemia. However, further research is needed on the specific protein expression and interaction relationships in the pathway.

Ethics statement

This experimental protocol has been reviewed and approved by the Animal Experimental Ethics Committee of Shanghai University of Traditional Chinese Medicine, with ethics approval number: PZSHUTCM211227011. The research was conducted in accordance with ethical standards, the Declaration of Helsinki and the related national and international guidelines.

Consent for publication

All data were generated in-house, and no paper mill was used. All authors agree to be accountable for all aspects of work ensuring integrity and accuracy.

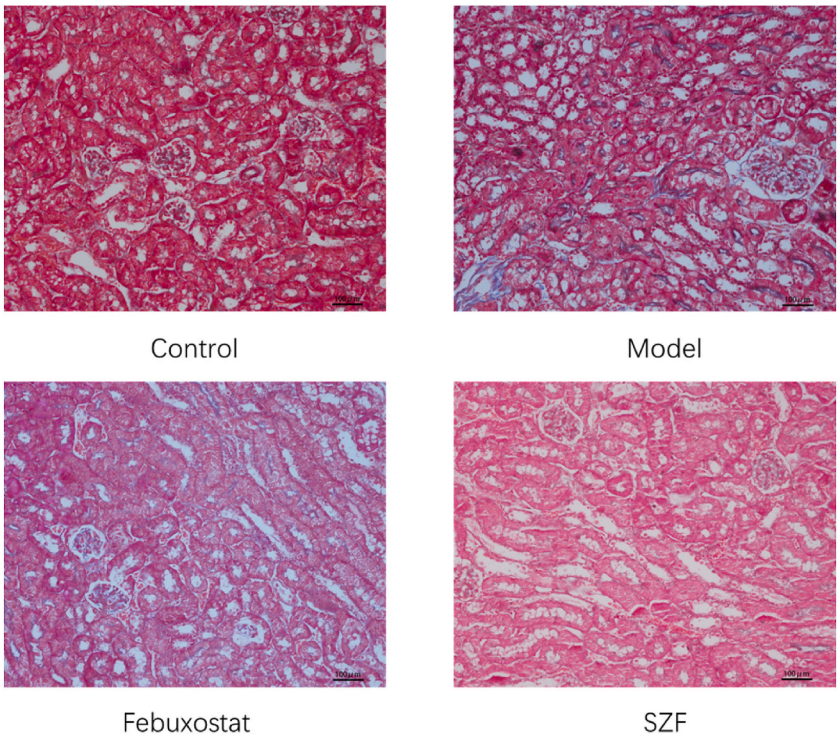

Fig. 19. Histomorphology of the Kidney (Masson, × 200). No signs of interstitial fibrosis were observed in the control group, Febuxostat group, or SZF group. In the model group, mild interstitial fibrosis was evident.

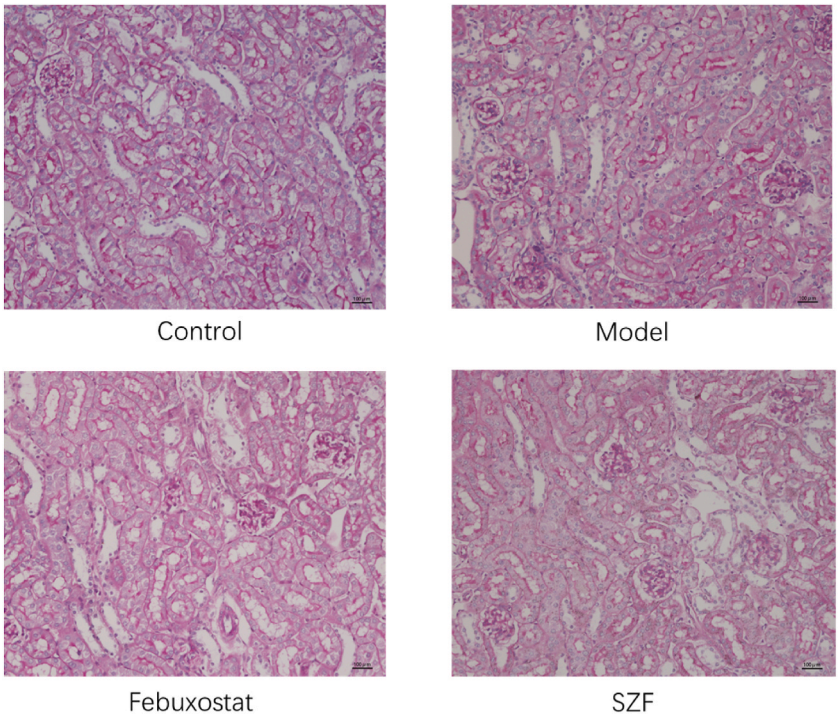

Fig. 20. Histomorphology of the Kidney (PAS, × 200). The control group showed no infiltration of inflammatory cells, and mesangial proliferation was absent. In the model group, interstitial inflammatory cell infiltration and mild mesangial proliferation were observed. The Febuxostat group and SZF group exhibited slight infiltration of inflammatory cells with no mesangial proliferation.

Table 8
Positive expression of Masson staining ($\bar{x} \pm s$, $n = 3$) .

Group	Quantity	Positive area (%)
Control	3	0.35 ± 0.12
Model	3	6.14 ± 1.17$^{\#\#\#\#}$
Febuxostat	3	0.64 ± 0.09****
SZF	3	0.77 ± 0.10****

Compared with the control, $^{\#}P < 0.05$, $^{\#\#}P < 0.01$, compared with the model , $^{*}P < 0.05$, $^{**}P < 0.01$, $^{***}P < 0.001$, $^{****}P < 0.0001$.

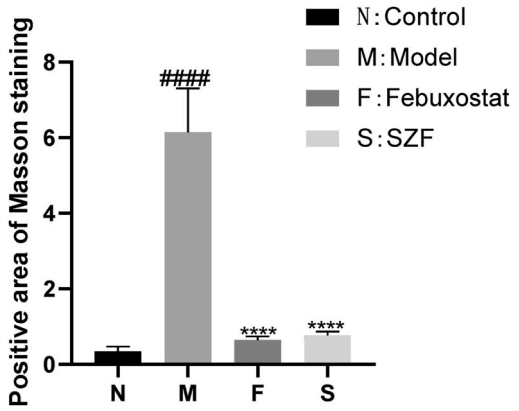

Fig. 21. Masson staining quantification results.

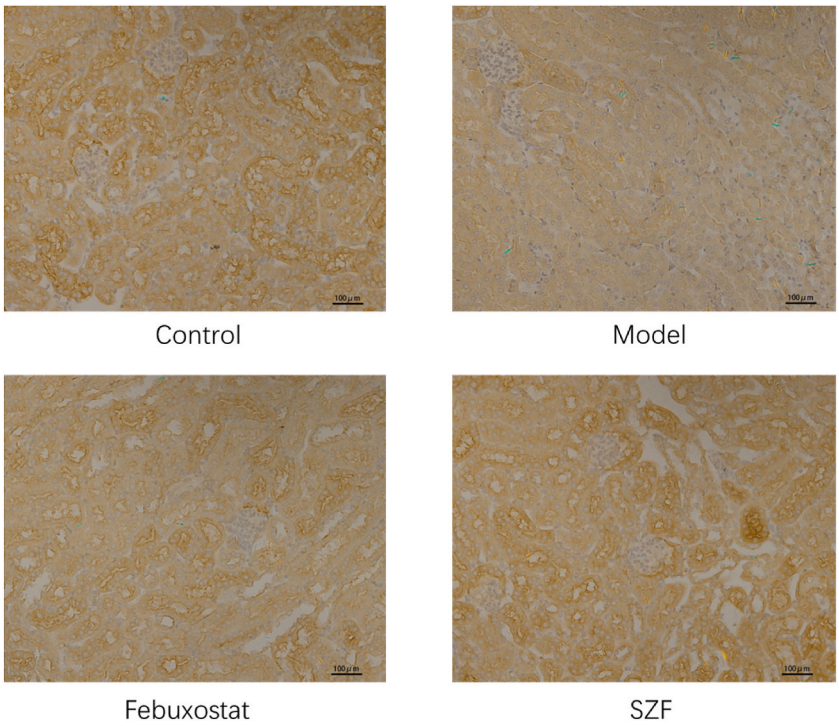

Fig. 22. Positive expression of Bcl-2 protein in mouse kidney (IHC , × 200) .

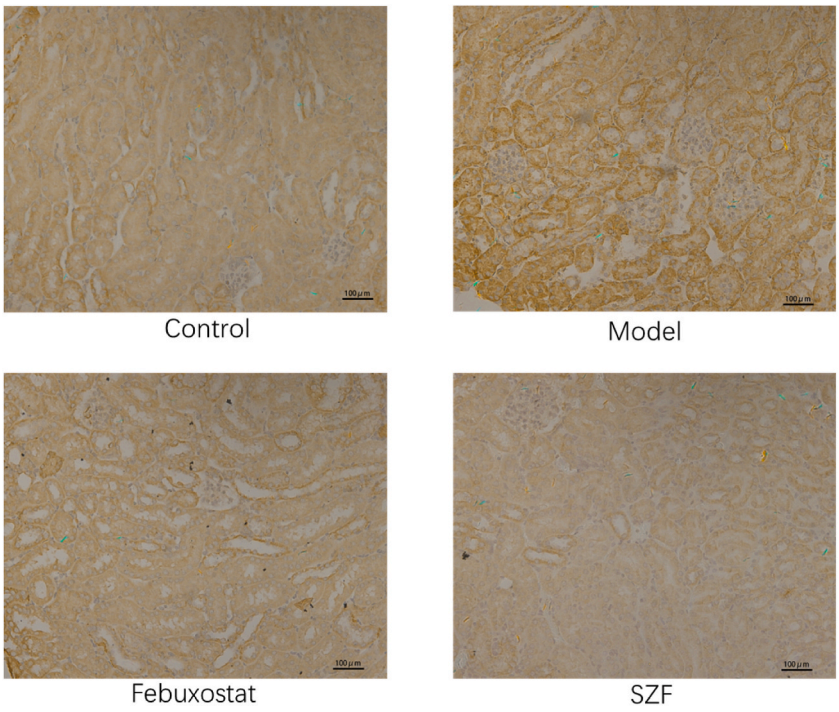

Fig. 23. Positive expression of Bax protein in mouse kidney (IHC, × 200) .

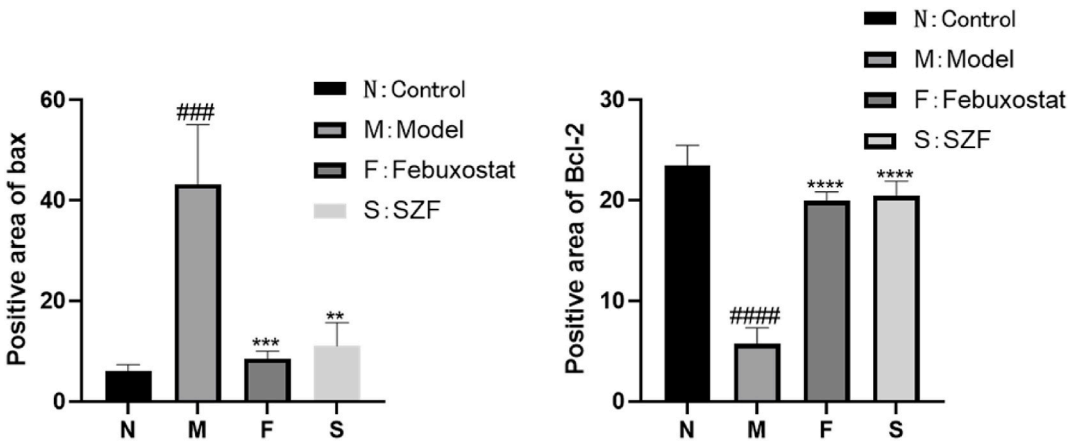

Fig. 24. Immunohistochemical quantification results.

Table 9
Positive expression of Bax and Bcl-2 protein in immunohistochemistry (% , $x \pm s$, $n = 3$) .

Group	Quantity	Bax	Bcl-2
Control	3	6.11 ± 1.20	23.46 ± 2.03
Model	3	43.24 ± 11.88$^{\#\#\#}$	5.74 ± 1.60$^{\#\#\#\#}$
Febuxostat	3	8.55 ± 1.46***	19.96 ± 0.88****
SZF	3	11.10 ± 4.61**	20.46 ± 1.45****

Compared with the control , $^{\#}P < 0.05$, $^{\#\#}P < 0.01$; compared with the model , $^{*}P < 0.05$, $^{**}P < 0.01$, $^{***}P < 0.001$, $^{****}P < 0.0001$.

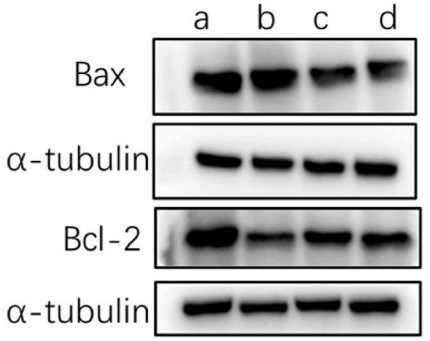

Fig. 25. Expression of Bax、Bcl-2 protein in mouse kidney
a: Control b: Model c: SZF d: Febuxostat.

Table 10
Expression of Bax and Bcl-2 protein in mouse kidney ($\bar{x} \pm s$, $n = 4$) .

Group	Quantity	Bax	Bcl-2
Control	4	0.8389 ± 0.1693	0.8927 ± 0.2330
Model	4	1.180 ± 0.09009$^{\#\#}$	0.5477 ± 0.2330$^{\#\#}$
SZF	4	0.7806 ± 0.1754***	0.8627 ± 0.1809***
Febuxostat	4	0.6709 ± 0.2518***	0.8533 ± 0.2378***

Compared with the control , $^{\#}P < 0.05$, $^{\#\#}P < 0.01$; Compared with the model , $^{**}P < 0.01$, $^{***}P < 0.001$.

Conflict of interest

The authors declare that they have no conflicts of interest.

Data availability statement

Date will be made available on request.

CRediT authorship contribution statement

Zhiyuan Wu: Writing – original draft, Data curation. **Chuanxu Wang:** Visualization, Validation, Data curation. **Feng Yang:** Visualization, Data curation. **Jiabao Zhou:** Visualization, Data curation. **Xuming Zhang:** Writing – review & editing. **Jiadong Xin:** Writing – review & editing. **Jiandong Gao:** Writing – review & editing, Supervision, Resources, Methodology, Funding acquisition.

Declaration of competing interest

We declare that the manuscript has not been submitted or accepted elsewhere. And all authors have reviewed and approved the final version of the manuscript. None of the authors has any financial arrangements with commercial companies that produce or sell products that have been used in this study.

Acknowledgments

This study was supported by the National Natural Science Foundation of China (81874437).

References

[1] N. Dalbeth, T.R. Merriman, L.K. Stamp, Gout [J], Lancet 388 (10055) (2016) 2039–2052, https://doi.org/10.1016/s0140-6736(16)00346-9.
[2] G. Bellomo, The relationship between uric acid, allopurinol, cardiovascular events, and kidney disease progression: a step forward [J], Am. J. Kidney Dis. : the official journal of the National Kidney Foundation 65 (4) (2015) 525–527, https://doi.org/10.1053/j.ajkd.2015.01.001.
[3] G. Li, C. Guan, L. Xu, L. Wang, C. Yang, L. Zhao, B. Zhou, C. Luo, H. Luan, W. Jiang, C. Li, Y. Xu, Scutellarin ameliorates renal injury via increasing CCN1 expression and suppressing NLRP3 inflammasome activation in hyperuricemic mice [J], Front. Pharmacol. 11 (2020) 584942, https://doi.org/10.3389/fphar.2020.584942.
[4] Z. Jia, W. Li, P. Bian, L. Yang, H. Liu, D. Pan, Z. Dou, Ursolic acid treats renal tubular epithelial cell damage induced by calcium oxalate monohydrate via inhibiting oxidative stress and inflammation [J], Bioengineered 12 (1) (2021) 5450–5461, https://doi.org/10.1080/21655979.2021.1955176.
[5] W.B. White, K.G. Saag, M.A. Becker, J.S. Borer, P.B. Gorelick, A. Whelton, B. Hunt, M. Castillo, L. Gunawardhana, Cardiovascular safety of febuxostat or allopurinol in patients with gout [J], N. Engl. J. Med. 378 (13) (2018) 1200–1210, https://doi.org/10.1056/NEJMoa1710895.

[6] L. Hua, S. Zhang, J. Yang, X. Zhou, S. Shi, Sanghuangporus vaninii ethanol extract alleviates hyperuricemic renal injury by regulating the uric acid transporters and inhibiting HK-2 apoptosis [J], Biomedicine & pharmacotherapy = Biomedecine & pharmacotherapie 164 (2023) 114970, https://doi.org/10.1016/j.biopha.2023.114970.
[7] G.Y. Tang, S. Li, Y. Xu, C. Zhang, X.Y. Xu, L. Xu, N. Wang, Y. Feng, Renal herb formula protects against hyperuricemic nephropathy by inhibiting apoptosis and inflammation [J], Phytomedicine 116 (2023) 154812, https://doi.org/10.1016/j.phymed.2023.154812.
[8] L. Yang, B. Wang, L. Ma, P. Fu, Traditional Chinese herbs and natural products in hyperuricemia-induced chronic kidney disease [J], Front. Pharmacol. 13 (2022) 971032, https://doi.org/10.3389/fphar.2022.971032.
[9] Y. Wu, Y. Wang, J. Ou, Q. Wan, L. Shi, Y. Li, F. He, H. Wang, L. He, J. Gao, Effect and Mechanism of ShiZhiFang on Uric Acid Metabolism in Hyperuricemic Rats [J]. Evidence-Based Complementary and Alternative Medicine, vol. 2018, eCAM, 2018 6821387, https://doi.org/10.1155/2018/6821387.
[10] Y. Wu, F. He, Y. Li, H. Wang, L. Shi, Q. Wan, J. Ou, X. Zhang, D. Huang, L. Xu, P. Lin, G. Yang, L. He, J. Gao, Effects of shizhifang on NLRP3 inflammasome activation and renal tubular injury in hyperuricemic rats [J], Evid. base Compl. Alternative Med. : eCAM 2017 (2017) 7674240, https://doi.org/10.1155/2017/7674240.
[11] J. Zhou, C. Wang, X. Zhang, Z. Wu, Y. Wu, D. Li, J. Gao, Shizhifang ameliorates pyroptosis of renal tubular epithelial cells in hyperuricemia through inhibiting NLRP3 inflammasome [J], J. Ethnopharmacol. 317 (2023) 116777, https://doi.org/10.1016/j.jep.2023.116777.
[12] Q. Li, P. Liu, C. Wu, L. Bai, Z. Zhang, Z. Bao, M. Zou, Z. Ren, L. Yuan, M. Liao, Z. Lan, S. Yin, L. Chen, Integrating network pharmacology and pharmacological validation to explore the effect of Shi Wei Ru Xiang powder on suppressing hyperuricemia [J], J. Ethnopharmacol. 298 (2022) 115679, https://doi.org/10.1016/j.jep.2022.115679.
[13] J. Ru, P. Li, J. Wang, W. Zhou, B. Li, C. Huang, P. Li, Z. Guo, W. Tao, Y. Yang, X. Xu, Y. Li, Y. Wang, L. Yang, TCMSP: a database of systems pharmacology for drug discovery from herbal medicines [J], J. Cheminf. 6 (2014) 13, https://doi.org/10.1186/1758-2946-6-13.
[14] H.Y. Xu, Y.Q. Zhang, Z.M. Liu, T. Chen, C.Y. Lv, S.H. Tang, X.B. Zhang, W. Zhang, Z.Y. Li, R.R. Zhou, H.J. Yang, X.J. Wang, L.Q. Huang, ETCM: an encyclopaedia of traditional Chinese medicine [J], Nucleic Acids Res. 47 (D1) (2019), https://doi.org/10.1093/nar/gky987. D976-d82.
[15] A. Daina, O. Michielin, V. Zoete, SwissTargetPrediction: updated data and new features for efficient prediction of protein targets of small molecules [J], Nucleic Acids Res. 47 (W1) (2019), https://doi.org/10.1093/nar/gkz382. W357-w64.
[16] Z. Liu, F. Guo, Y. Wang, C. Li, X. Zhang, H. Li, L. Diao, J. Gu, W. Wang, D. Li, F. He, BATMAN-TCM: a bioinformatics analysis Tool for molecular mechANism of traditional Chinese medicine, Sci. Rep. 6 (2016) 21146, https://doi.org/10.1038/srep21146.
[17] D. Szklarczyk, R. Kirsch, M. Koutrouli, K. Nastou, F. Mehryary, R. Hachilif, A.L. Gable, T. Fang, N.T. Doncheva, S. Pyysalo, P. Bork, L.J. Jensen, C. VON Mering, The STRING database in 2023: protein-protein association networks and functional enrichment analyses for any sequenced genome of interest [J], Nucleic Acids Res. 51 (D1) (2023), https://doi.org/10.1093/nar/gkac1000. D638-d46.
[18] UniProt, The universal protein knowledgebase in 2023 [J], Nucleic Acids Res. 51 (D1) (2023), https://doi.org/10.1093/nar/gkac1052. D523-d31.
[19] M. Safran, N. Rosen, M. Twik, R. Barshir, T.I. Stein, D. Dahary, S. Fishilevich, D. Lancet, The GeneCards Suite [M], Practical Guide to Life Science Databases, 2021, pp. 27–56.
[20] J. PiñERO, J.M. RamíREZ-Anguita, J. SaüCH-Pitarch, F. Ronzano, E. Centeno, F. Sanz, L.I. Furlong, The DisGeNET knowledge platform for disease genomics: 2019 update, Nucleic Acids Res. 48 (D1) (2019) D845–D855.
[21] B.T. Sherman, M. Hao, J. Qiu, X. Jiao, M.W. Baseler, H.C. Lane, T. Imamichi, W. Chang, DAVID: a web server for functional enrichment analysis and functional annotation of gene lists (2021 update), Nucleic Acids Res. 50 (W1) (2022) W216–W221, https://doi.org/10.1093/nar/gkac194.
[22] M. Tao, Y. Shi, L. Tang, Y. Wang, L. Fang, W. Jiang, T. Lin, A. Qiu, S. Zhuang, N. Liu, Blockade of ERK1/2 by U0126 alleviates uric acid-induced EMT and tubular cell injury in rats with hyperuricemic nephropathy [J], Am. J. Physiol. Ren. Physiol. 316 (4) (2019) F660–F673, https://doi.org/10.1152/ajprenal.00480.2018.
[23] M.Y. Ansari, K. Novak, T.M. Haqqi, ERK1/2-mediated activation of DRP1 regulates mitochondrial dynamics and apoptosis in chondrocytes [J], Osteoarthritis Cartilage 30 (2) (2022) 315–328, https://doi.org/10.1016/j.joca.2021.11.003.
[24] R. Sugiura, R. Satoh, T. Takasaki, ERK: a double-edged sword in cancer. ERK-Dependent apoptosis as a potential therapeutic strategy for cancer [J], Cells 10 (10) (2021), https://doi.org/10.3390/cells10102509.
[25] P. Thongnuanjan, S. Soodvilai, S. Fongsupa, N. Chabang, P. Vivithanaporn, P. Tuchinda, S. Soodvilai, Protective effect of panduratin A on cisplatin-induced apoptosis of human renal proximal tubular cells and acute kidney injury in mice [J], Biol. Pharmaceut. Bull. 44 (6) (2021) 830–837, https://doi.org/10.1248/bpb.b21-00036.
[26] H. Rizwan, S. Pal, S. Sabnam, A. Pal, High Glucose Augments ROS Generation Regulates Mitochondrial Dysfunction and Apoptosis via Stress Signalling Cascades in Keratinocytes [J], vol. 241, Life sciences, 2020 117148, https://doi.org/10.1016/j.lfs.2019.117148.
[27] J.Y. Choe, K.Y. Park, S.K. Kim, Oxidative stress by monosodium urate crystals promotes renal cell apoptosis through mitochondrial caspase-dependent pathway in human embryonic kidney 293 cells: mechanism for urate-induced nephropathy [J], Apoptosis : an international journal on programmed cell death 20 (1) (2015) 38–49, https://doi.org/10.1007/s10495-014-1057-1.
[28] A.B. Sanz, B. SantamaríA, M. Ruiz-Ortega, J. Egido, A. Ortiz, Mechanisms of renal apoptosis in health and disease [J], J. Am. Soc. Nephrol. 19 (9) (2008) 1634–1642, https://doi.org/10.1681/asn.2007121336.
[29] N. Liu, L. Xu, Y. Shi, L. Fang, H. Gu, H. Wang, X. Ding, S. Zhuang, Pharmacologic targeting ERK1/2 attenuates the development and progression of hyperuricemic nephropathy in rats [J], Oncotarget 8 (20) (2017) 33807–33826, https://doi.org/10.18632/oncotarget.16995.
[30] Y. Shi, L. Xu, M. Tao, L. Fang, J. Lu, H. Gu, S. Ma, T. Lin, Y. Wang, W. Bao, A. Qiu, S. Zhuang, N. Liu, Blockade of enhancer of zeste homolog 2 alleviates renal injury associated with hyperuricemia, Am. J. Physiol. Ren. Physiol. 316 (3) (2019) F488–F505, https://doi.org/10.1152/ajprenal.00234.2018.
[31] Y. Wu, L. Wang, D. Deng, Q. Zhang, W. Liu, Renalase protects against renal fibrosis by inhibiting the activation of the ERK signaling pathways [J], Int. J. Mol. Sci. 18 (5) (2017), https://doi.org/10.3390/ijms18050855.
[32] Y. Zou, C. Yu, Q. Huang, X. Tan, X. Tan, X. Zhu, D. Yi, J. Mao, Investigating the active chemical constituents and pharmacology of Nanocnide lobata in the treatment of burn and scald injuries [J], PLoS One 18 (6) (2023) e0287147, https://doi.org/10.1371/journal.pone.0287147.